

## APPLICATION OF A MULTIPHASE FLOW MODEL FOR SIMULATIONS OF NAPL BEHAVIOR AT INCLINED MATERIAL INTERFACES

JIŘÍ MIKYŠKA<sup>1</sup> AND TISSA ILLANGASEKARE<sup>2</sup>

**Abstract.** Multiphase models that simulate the behavior of non-aqueous phase liquids (NAPL's) in porous media can be used to obtain fundamental understanding of the complex behavior and predict the fate of waste chemicals in the subsurface. Existing models have limitations in simulating highly heterogeneous systems to be able to represent realistic field conditions. This document reports development of a new multiphase flow code called VODA. It starts with a brief introduction of the mathematical model of the multiphase flow in porous media. Then, the Control Volume Finite Element (CVFE) discretization is described and finally, examples of several two-phase flow computations in heterogeneous media are also given.

**Key words.** finite element method, multiphase flow, NAPL, heterogeneous medium, inclined interface

**AMS subject classifications.** 35M10, 65M12, 65M60

**1. Mathematical Model.** The basic equations describing the multiphase flow in porous media are developed from the Darcy laws and continuity equations for all phases, cf [13], [10]:

$$(1.1) \quad \frac{\partial(\phi\rho_\alpha S_\alpha)}{\partial t} + \nabla \cdot (\rho_\alpha v_\alpha) = \rho_\alpha q_\alpha, \quad \alpha \in \{w, n\}$$

$$(1.2) \quad v_\alpha = -\frac{k_{r\alpha}}{\mu_\alpha} \mathbf{K} \cdot (\nabla p_\alpha - \rho_\alpha g), \quad \alpha \in \{w, n\}$$

$$(1.3) \quad k_{r\alpha} = k_{r\alpha}(S_\alpha), \quad \alpha \in \{w, n\}$$

$$(1.4) \quad p_c = p_c(S_w) = p_n - p_w, \quad S_w + S_n = 1.$$

In these equations  $\phi$  denotes porosity,  $\rho_\alpha$  is the density of phase  $\alpha$ ,  $S_\alpha$  are the phase saturations,  $v_\alpha$  denote the Darcy velocities of the respective phases,  $q_\alpha$  is the source/sink term for  $\alpha$ -phase,  $\mathbf{K}$  stands for intrinsic medium permeability tensor,  $k_{r\alpha}$  are the relative permeabilities of the respective phases,  $\mu_\alpha$  are the viscosities of water and NAPL-phases, and finally,  $p_c$  denotes capillary pressure.

We use the following form of the equations - the so-called pressure-saturation formulation of the multiphase flow equations that uses the water pressure  $p_w$  and nonwetting phases saturations  $S_\alpha$  as primary variables:

$$(1.5) \quad \frac{\partial(\phi\rho_w(1 - S_n))}{\partial t} = \nabla \cdot \left[ \rho_w \frac{k_{rw}}{\mu_w} \mathbf{K} \cdot (\nabla p_w - \rho_w g) \right] + \rho_w q_w$$

$$(1.6) \quad \frac{\partial(\phi\rho_n S_n)}{\partial t} = \nabla \cdot \left[ \rho_n \frac{k_{rn}}{\mu_n} \mathbf{K} \cdot (\nabla p_w + \nabla p_c - \rho_n g) \right] + \rho_n q_n.$$

<sup>1</sup>Department of Mathematics, Faculty of Nuclear Sciences and Physical Engineering, Czech Technical University in Prague, Trojanova 13, 120 00 Prague, Czech Republic.

<sup>2</sup>Department of Environmental Science and Engineering, Colorado School of Mines, Golden, Colorado, CO 80401, USA.

Capillary pressure is described by the Brooks-Corey model

$$p_c(S_w) = p_d S_e^{-\frac{1}{\lambda}},$$

where the parameter  $p_d$  denotes the entry pressure and  $\lambda$  is the pore size distribution index. In both relations above,  $S_e$  denotes the effective saturation given by

$$S_e = \frac{S_w - S_{wr}}{1 - S_{wr}},$$

where  $S_{wr}$  is the residual wetting phase saturation.

The Brooks-Corey capillary pressure relationships are used in conjunction with the following Burdine theorem for the relative permeabilities:

$$(1.7) \quad k_{rw}(S_w) = (S_e)^{\frac{2+3\lambda}{\lambda}},$$

$$(1.8) \quad k_{rn}(S_w) = (1 - S_e)^2 \cdot (1 - S_e^{\frac{2+\lambda}{\lambda}}),$$

These equations are to be solved in a bounded spatial domain  $\Omega \in \mathbb{R}^2$  and time interval  $I = \langle 0, T \rangle, T > 0$ . The system must be completed with initial and boundary conditions as follows

$$(1.9) \quad S_n(x, 0) = S_n^{Ini}(x) \quad \forall x \in \Omega,$$

$$(1.10) \quad p_w(x, t) = p_w^{Dir}(x, t), \quad S_n(x, t) = S_n^{Dir}(x, t) \quad \forall x \in \partial\Omega_{Dir}, \forall t \in I,$$

$$(1.11) \quad v_w(x, t) = v_w^{Neu}(x, t), \quad v_n(x, t) = v_n^{Neu}(x, t) \quad \forall x \in \partial\Omega_{Neu}, \forall t \in I,$$

where  $\partial\Omega_{Dir}$  and  $\partial\Omega_{Neu}$  is a decomposition of the boundary  $\partial\Omega$ .

Note, that the capillary pressure-saturation and relative permeability-saturation relationships can be different in the different positions. This point is extremely important especially in the case of the Brooks-Corey relationships, which accounts for nonzero entry pressures, and is thus suitable for description of the entry pressure effects at the material interfaces.

**2. Interface conditions.** Special attention is paid to the NAPL's behavior at sharp material interfaces. Note, that the model equations 1.2 are valid only in the regions where the model coefficients (as  $K$ ,  $p_d$ ,  $\lambda$  etc) are smooth. At the sharp material heterogeneities, these coefficients are discontinuous, and thus some interface conditions must be imposed. These conditions were throughoughly examined in [8, 1] in detail.

Assume a sharp interface between two sands 1 and 2, with two different retention curves, see Figure 2.1. The first condition at the heterogeneity is the mass conservation law across the interface. The second condition says that the capillary pressure should be continuous whenever it is possible, i.e. if the non-wetting phase saturation is such that the non-wetting phase pressure in sand 1 is greater than the entry pressure in sand 2. Otherwise, the non-wetting phase pressure must necessarily be discontinuous and no NAPL can pass through the interface. Non-wetting phase saturation at the interface in sand 2 is then zero. From Figure 2.1 we can deduce that the interface acts as a barrier unless the non-wetting phase saturation is high enough (namely  $1 - S_{crit}$  in Figure 2.1) and if the NAPL is pushed from sand 1 to sand 2. If the NAPL is pushed in the opposite direction then the non-wetting phase pressure can be made continuous at any time and no barrier effect takes place.

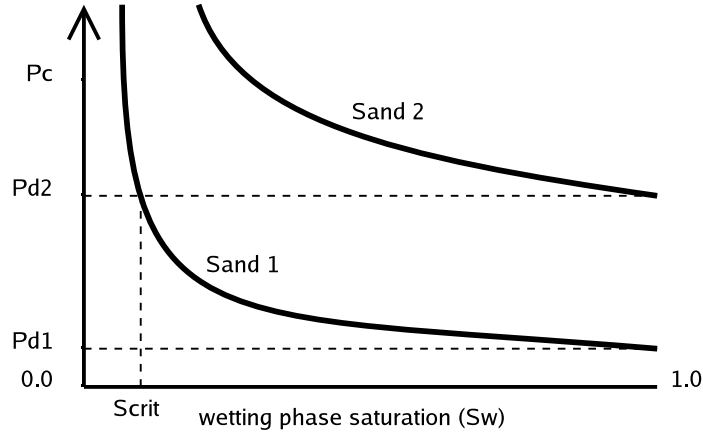


FIG. 2.1. Capillary pressure - saturation relations at an interface between two sands

**3. Discretization.** All modern numerical techniques are based on a weak formulation of the solved equations. This can be obtained using the well established procedure - multiplying the equations by a weighting function  $W$ , integrating the equations over  $\Omega$  and applying Green's theorem results in the following weak form:

$$(3.1) \quad \int_{\Omega} W \frac{\partial(\phi \rho_{\alpha} S_{\alpha})}{\partial t} dx + \int_{\Omega} \rho_{\alpha} \lambda_{\alpha} \nabla W \cdot K \cdot (\nabla p_w + \delta_{\alpha n} \nabla p_c - \rho_{\alpha} g) dx \\ = \int_{\partial \Omega_{Neu}} W \rho_{\alpha} v_{\alpha}^{Neu} dS + \int_{\Omega} W \rho_{\alpha} q_{\alpha} dx, \quad \alpha \in \{w, n\}$$

where  $\lambda_{\alpha} = \frac{k_{\alpha}}{\mu_{\alpha}}$  is the phase  $\alpha$  mobility coefficient. Based on this weak form we will develop the control volume finite element discretizations of the multiphase flow equations.

This approach follows [9, 10]. Having covered the domain  $\Omega$  by a triangulation and denoting the linear basis functions corresponding to the triangulation by  $N_i$ , the following CVFE-scheme can be derived for  $\alpha \in \{w, n\}$

$$(-1)^{\delta_{\alpha w}} \frac{[\phi \rho_{\alpha} S_n]_i^{n+1} - [\phi \rho_{\alpha} S_n]_i^n}{\Delta t} V_i + \sum_{j \in \eta_i} \lambda_{\alpha ij} \rho_{\alpha} \gamma_{\alpha ij} (\psi_{\alpha j}^{n+1} - \psi_{\alpha i}^{n+1}) = \\ = (\rho_{\alpha i} q_{\alpha i})^{n+1} V_i + m_{\alpha i}^{n+1},$$

where  $m_{\alpha i}^{n+1} = \int_{\partial \Omega_{Neu}} N_i \rho_{\alpha} v_{\alpha}^{Neu} dS$  is the linear finite element discretization of the Neumann-boundary-condition term,  $\psi_{\alpha i}^{n+1} = p_{wi}^{n+1} + \delta_{\alpha n} p_{ci}^{n+1} - \rho_{\alpha} g_i$ , and  $\gamma_{\alpha ij} = -\int_{\Omega} \nabla N_i \cdot K \cdot \nabla N_j dx$  is the finite-element stiffness matrix. Note, that all values at the right hand side are taken in time  $n+1$ , and thus the CVFE scheme is fully implicit. Furthermore, the mobility coefficient between nodes  $i$  and  $j$  are chosen as the mobility in the upwind node in the sense:

$$(3.2) \quad \lambda_{\alpha ij} = \begin{cases} \lambda_{\alpha i} & \text{if } \gamma_{ij}(\psi_{\alpha j} - \psi_{\alpha i}) \leq 0 \\ \lambda_{\alpha j} & \text{if } \gamma_{ij}(\psi_{\alpha j} - \psi_{\alpha i}) > 0 \end{cases}$$

Finally,  $\Delta t$  denotes the timestep, and  $V_i = \int_{\Omega} N_i dx$  is a weighting factor.

**4. Numerical treatment of the interface effects.** In view of applications of our model to NAPL behavior in heterogeneous media it is very important to handle the interface effects in a physically correct manner. The CVFE-model simulates the dam effect correctly (due to upwinding of the mobility coefficients) assumed that no mesh nodes are present at the interface. In this case, if the non-wetting phase pressure is not sufficient to pass the interface, then the upwind-taken mobility is zero and no non-wetting phase flux across the interface occurs. Unfortunately, the library, which was used for model implementation, aligns automatically mesh nodes with the subdomains interfaces and it is not possible to switch off this option. For this reason, it was necessary to assign a subdomain number to every node. If a node is an interior node of a subdomain, it shares its number. For the nodes at the subdomain interfaces the assignment is done in such way that the node belongs to the subdomain with the highest entry pressure. For the evaluation of the capillary pressure at a node at the interface, capillary pressure-saturation relationship which corresponds to the subdomain number assigned to the node is used instead of the subdomain assigned to the current element. Then the entry pressure effects are simulated in a physically correct way.

**5. Application: NAPL flow on an inclined layer.** The CVFE scheme was implemented into a new multiphase flow package called VODA. For implementation we used the software package UG, which is a C library for development of numerical codes currently developed at the University of Heidelberg (see [17, 2, 4]). VODA can solve two- and three-phase equations in 2-D using the CVFE discretization on triangular unstructured meshes. The non-linear discrete equations are linearized using the Newton method with linesearch option. Linear systems are solved using a linear multigrid solver based on the BiCGStab method. The code was tested on two one-dimensional problems for which quasianalytic solutions were available - i.e. McWhorter-Sunada and Buckley-Leverett problems, see [14, 6, 15, 3] for details on the McWhorter-Sunada problem, e.g. [7, 11] for details on the Buckley-Leverett problem and [12] for details on results of the convergence analysis that were computed using VODA.

In this section we will examine flow of water and oil on inclined layers. Domain  $\Omega \subset \mathbb{R}^2$  is a rectangle  $27.8 \times 14.3$  cm with a small square hole ( $1 \times 1$  cm) inside, which serves as a source zone for NAPL spill. This domain is occupied by two different sands. Sands and fluids properties are summarized in Tables 5.1 and 5.2.

Property [units]	Sand # 1 (upper layer)	Sand # 2 (lower layer)
Intrinsic permeability $K$ [ $\text{m}^2$ ]	$1.43 \cdot 10^{-10}$	$1.173 \cdot 10^{-12}$
Porosity $\phi$ [-]	0.48	0.37
Entry pressure $p_d$ height [m]	0.3437	0.6953
Brooks-Corey index $\lambda$ [-]	5.85	7.26
Residual water saturation [-]	0.16	0.22
Residual NAPL saturation [-]	0.20	0.21

TABLE 5.1  
*Sands properties*

The sharp interface between the two sands is inclined with grades 1%, 5%, and 10%. The domains and the triangulations aligned with the interface used are illustrated in Figure 5.4. The NAPL is introduced into the system through the left, right, and bottom edges of the source zone where a given boundary flux is prescribed. The top edge of the source zone is impermeable and this is also valid for the top and bot-

Property [units]	Water	NAPL (PCE)
Density $\rho$ [ $\text{kg m}^{-3}$ ]	1000	1630
Viscosity $\mu$ [ $\text{kg m}^{-1}\text{s}^{-1}$ ]	0.001	$8.802 \cdot 10^{-4}$

TABLE 5.2  
Fluids properties

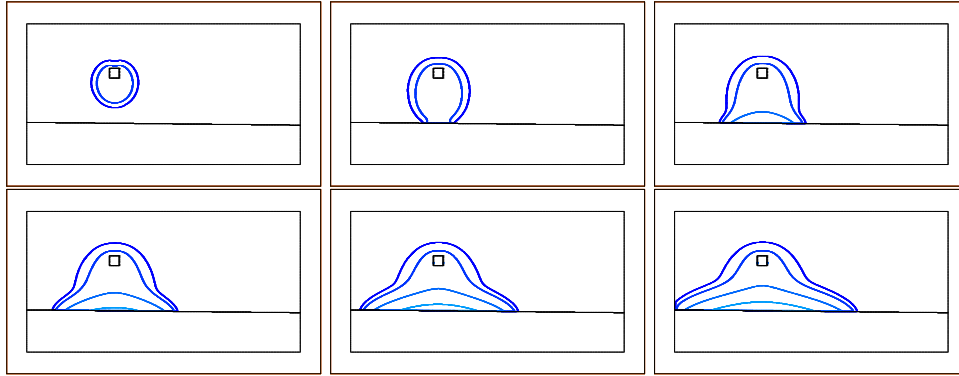


FIG. 5.1. Evolution of the NAPL spill at times from 10 minutes to 60 minutes (from left to right, top to bottom) at the material interface, 1% grade. NAPL saturation isolines are shown (1% the darkest one, increasing by 5%).

tom outer boundary edges of domain  $\Omega$ . The left and right outer boundary edges are Dirichlet edges with prescribed zero NAPL saturation and hydrostatic water pressure. At the beginning, the water pressure is hydrostatic (i.e. no flow) in whole domain and no NAPL phase is present. We simulate time evolution of this system with special attention for the interface effects, which are caused by different entry pressures in the sands.

Figures 5.1–5.3 illustrate evolution of the systems and entry pressure effects in 10 minute intervals up to 60 minutes after the beginning of the spill. The timestep used is 30 seconds in all cases. From Figures 5.1–5.3 one can see that the NAPL saturation is never so high so that the NAPL could penetrate through the interface regardless of the interface slope.

Every problem was solved on the respective mesh shown in Figure 5.4 and on its four regular refinement. We present the final states of the NAPL spill after 60 minutes from the initial time computed on the original mesh (as shown in Figure 5.4) and on its level 2 and level 4 refinements. Comparison of these results allows us to see the convergence of the numerical scheme in situations when no analytical solution is known. If the mesh is fine enough the differences between solutions obtained on further refined mesh tend to be very small if ever visible (compare e.g. results obtained on level 2 and level 4 refinement).

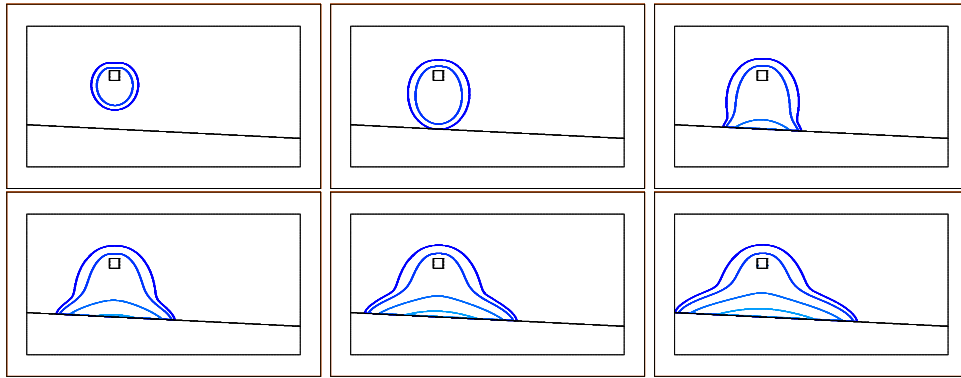


FIG. 5.2. Evolution of the NAPL spill at times from 10 minutes to 60 minutes (from left to right, top to bottom) at the material interface, 5% grade. NAPL saturation isolines are shown (1% the darkest one, increasing by 5%).

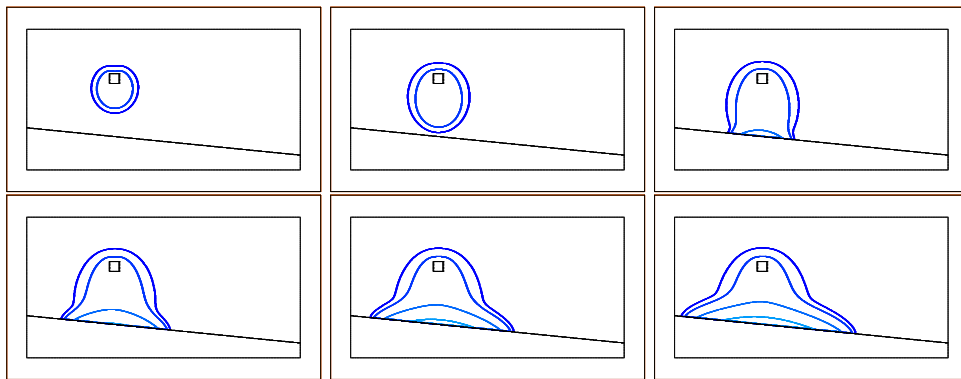


FIG. 5.3. Evolution of the NAPL spill at times from 10 minutes to 60 minutes (from left to right, top to bottom) at the material interface, 10% grade. NAPL saturation isolines are shown (1% the darkest one, increasing by 5%).

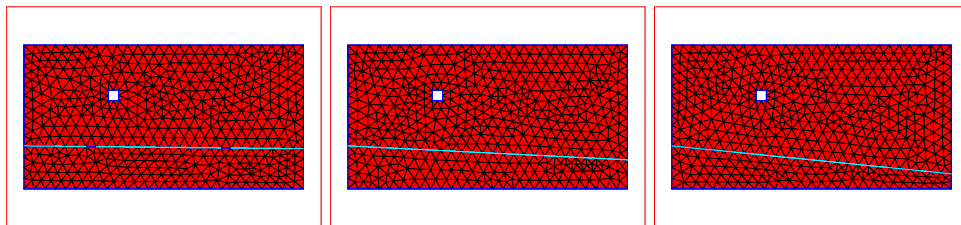


FIG. 5.4. Domains  $\Omega$ 's and the triangulations used (1%, 5%, and 10% grades).

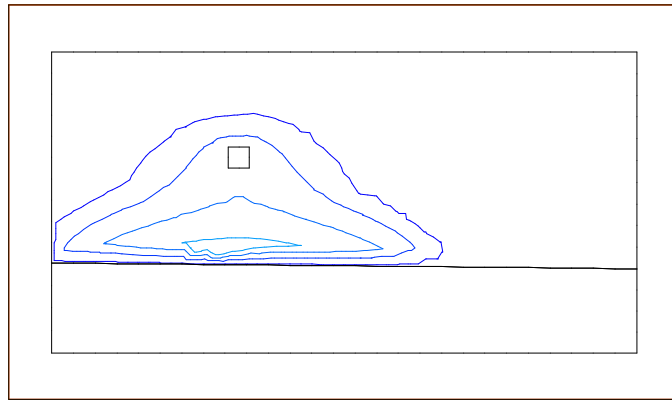


FIG. 5.5. NAPL spill at time 60 minutes, interface grade 1%, mesh in Figure 5.4 left. NAPL saturation isolines are shown (1% the darkest one, increasing by 5%).

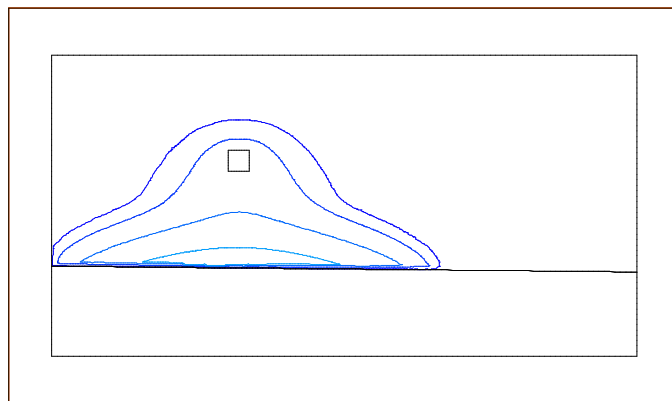


FIG. 5.6. NAPL spill at time 60 minutes, interface grade 1%, 2 regular refinements of the mesh in Figure 5.4 left. NAPL saturation isolines are shown (1% the darkest one, increasing by 5%).

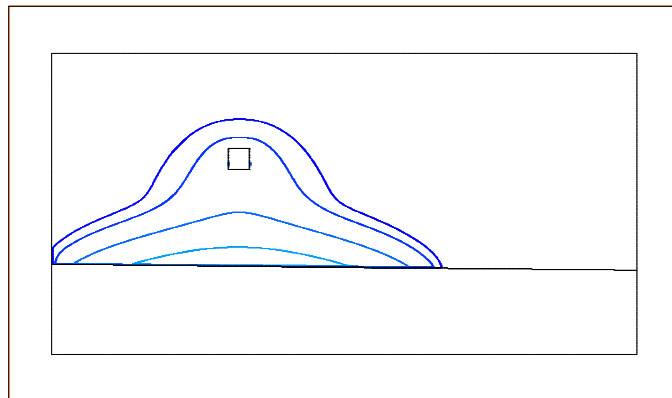


FIG. 5.7. NAPL spill at time 60 minutes, interface grade 1%, 4 regular refinements of the mesh in Figure 5.4 left. NAPL saturation isolines are shown (1% the darkest one, increasing by 5%).

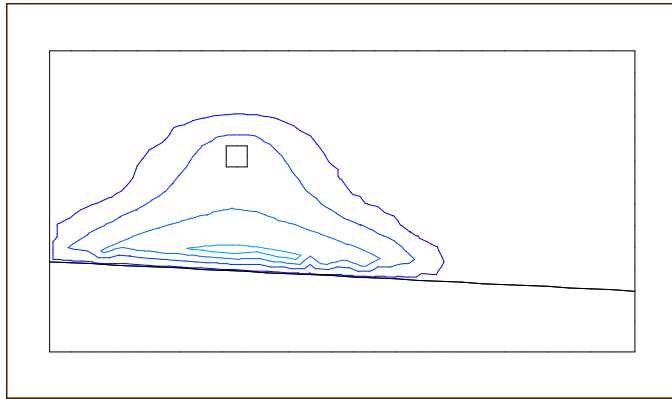


FIG. 5.8. NAPL spill at time 60 minutes, interface grade 5%, computed on the mesh in Figure 5.4 middle. NAPL saturation isolines are shown (1% the darkest one, increasing by 5%).

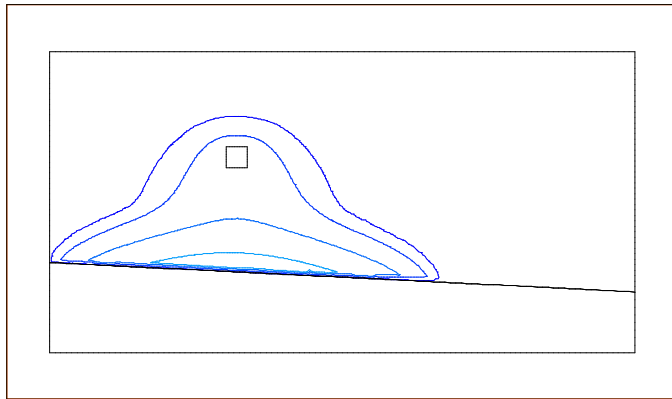


FIG. 5.9. NAPL spill at time 60 minutes, interface grade 5%, 2 regular refinements of the mesh in Figure 5.4 middle. NAPL saturation isolines are shown (1% the darkest one, increasing by 5%).

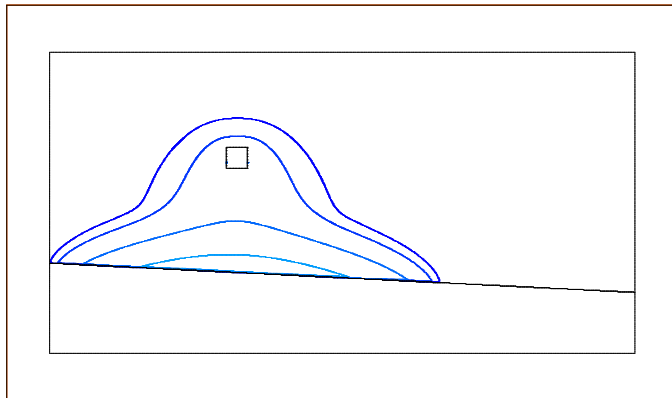


FIG. 5.10. NAPL spill at time 60 minutes, interface grade 5%, 4 regular refinements of the mesh in Figure 5.4 middle. NAPL saturation isolines are shown (1% the darkest one, increasing by 5%).

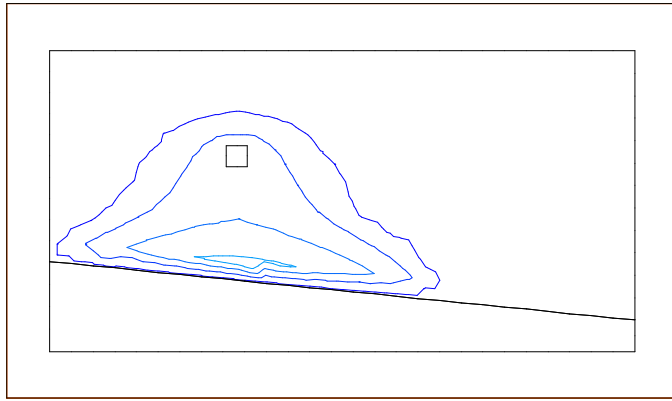


FIG. 5.11. NAPL spill at time 60 minutes, interface grade 10%, computed on the mesh in Figure 5.4 right. NAPL saturation isolines are shown (1% the darkest one, increasing by 5%).

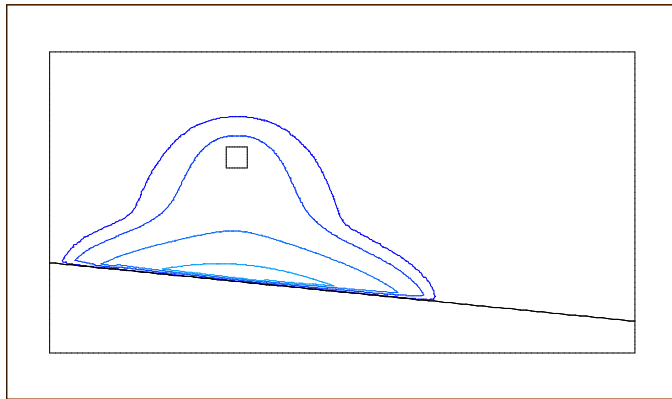


FIG. 5.12. NAPL spill at time 60 minutes, interface grade 10%, 2 regular refinements of the mesh in Figure 5.4 right. NAPL saturation isolines are shown (1% the darkest one, increasing by 5%).

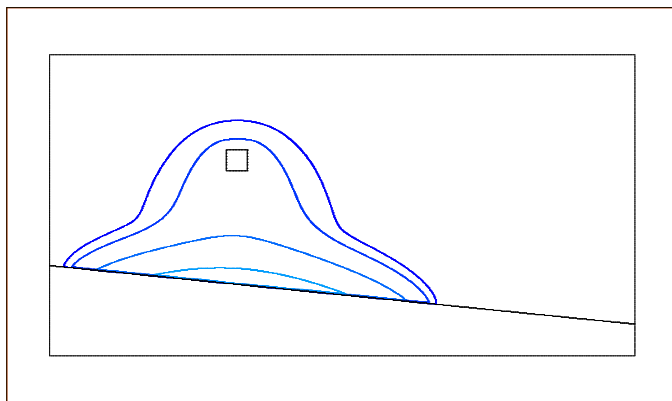


FIG. 5.13. NAPL spill at time 60 minutes, interface grade 10%, 4 regular refinements of the mesh in Figure 5.4 right. NAPL saturation isolines are shown (1% the darkest one, increasing by 5%).

**6. Conclusion.** Results of these computations are important for verification of the new multiphase flow code. Analytical solutions for two-phase flow are available for one-dimensional horizontal flow through homogeneous sands only. As our research aims to investigation of the NAPL behavior at sharp material interfaces we need to test our model on situations involving heterogeneous media. For this purpose several examples were computed in which the material interfaces were inclined with different grades. The results show that the model is able to capture the entry pressure effects in a physically correct way. The computations were repeated on a set of gradually refined meshes (up to level 4 regular refinement) and it is possible to observe that the computational results do not change much when the mesh is refined already from the second level of the refinement. This is a good indication of the correct function of the model in more complex situation than is required by known analytical solutions.

**Acknowledgements.** The first author was partly supported by the project "Applied Mathematics in Technology and Physics" MSM 6840770010 of the Ministry of Education of the Czech Republic. Partial funding for the research of the second author was provided by the National Science Foundation through the award 0222286 (CMG RESEARCH: "Numerical and Experimental Validation of Stochastic Upscaling for Subsurface Contamination Problems Involving Multiphase Volatile Chlorinated Solvents" [16]). Participation in this seminar was possible due to the support of the Internal Grant of the Czech Technical University in Prague, No. 0415314.

## REFERENCES

- [1] P. BASTIAN. Numerical computation of multiphase flow in porous media. Habilitationsschrift, 1999.
- [2] P. BASTIAN, K. BIRKEN, S. LANG, K. JOHANNSEN, N. NEUSS, H. RENTZ-REICHERT, AND C. WIENERS. UG: A flexible software toolbox for solving partial differential equations. *Computing and Visualization in Science*, 1:27–40, 1997.
- [3] M. BENEŠ, R. FUČÍK, J. MIKYŠKA, AND T. H. ILLANGASEKARE. Generalization of the benchmark solution for the two-phase flow. In Karel Kovář, Zbyněk Hrkal, and Jirí Bruthans, editors, *FEM-MODFLOW 2004*, pages 181–184, Karlovy Vary, Czech Republic, 2004.
- [4] P. BASTIAN, K. JOHANNSEN, AND V. REICHENBERGER. *UG Tutorial*, 1999.
- [5] M. BENEŠ, M. STÝBLO, J. MARYŠKA, AND J. MUŽÁK. The application of mathematical models of the transport of chemical substances in the remediation of consequences of the uranium mining. In *Proceedings of 3rd Workshop on Modelling of Chemical Reaction Systems*, Heidelberg, July 1996. ISBN 3-932217-00-4.
- [6] Z. X. CHEN, G. S. BODVARSON, AND P. A. WITHERSPOON. Comment on "exact integral solution for two-phase flow" by David B. McWhorter and Daniel K. Sunada. *Water Resources Research*, 28(5):1477–1478, May 1992.
- [7] R. E. COLLINS. *Flow of Fluids through Porous Materials*. The Petroleum Publishing Company, Tulsa, 1976.
- [8] M. I. DE NEEF AND J. MOLENAAR. Analysis of DNAPL infiltration in a medium with a low-permeable lens. *Computational Geosciences*, 1:191–214, 1997.
- [9] P. A. FORSYTH. A control volume finite element approach to NAPL groundwater contamination. *SIAM J. Sci. Stat. Comput.*, 12(5):1029–1057, September 1991.
- [10] R. HELMIG. *Multiphase Flow and Transport Processes in the Subsurface : A Contribution to the Modeling of Hydrosystems*. Springer verlag, Berlin, 1997.
- [11] P. S. HUYAKORN AND G. F. PINDER. *Computational Methods in Subsurface Flow*. Academic Press, New York, 1983.
- [12] J. MIKYŠKA, M. BENEŠ, T. H. ILLANGASEKARE, AND A. TURNER. Development and validation of a multiphase flow model for applications in NAPL behaviour in highly heterogeneous aquifer formations. In Karel Kovář, Zbyněk Hrkal, and Jirí Bruthans, editors, *FEM-MODFLOW 2004*, pages 215–218, Karlovy Vary, Czech Republic, 2004.
- [13] J. MIKYŠKA. First steps towards formulation of surfactant enhanced NAPL dissolution problem. Technical report, Department of Mathematics, FNSPE CTU in Prague, Preprints MMG 1-02, 2002.

- [14] D. B. MCWHORTER AND D. K. SUNADA. Exact integral solutions for two-phase flow. *Water Resources Research*, 26(3):399–413, 1990.
- [15] D. B. MCWHORTER AND D. K. SUNADA. Reply. *Water Resources Research*, 28(5):1479, May 1992.
- [16] Center for Experimental Study of Subsurface Environmental Processes (CESEP), Colorado School of Mines, Golden, Colorado. <http://cesep.mines.edu>.
- [17] UG homepage. <http://cox.iwr.uni-heidelberg.de/~ug/>.